remote sensing

MDPI

Article

Aboveground Forest Biomass Estimation Combining L- and P-Band SAR Acquisitions

Michael Schlund [1,*] and Malcolm W. J. Davidson [2]

1 Cartography, GIS & Remote Sensing Department, Institute of Geography, Georg-August-University Göttingen, Goldschmidtstr. 5, 37077 Göttingen, Germany

2 European Space Research and Technology Centre, European Space Agency, 2200 AG Nordwijk, The Netherlands; malcolm.davidson@esa.int

* Correspondence: michael.schlund@uni-goettingen.de; Tel.: +49-551-3-97979

Received: 8 June 2018; Accepted: 19 July 2018; Published: 20 July 2018

Abstract: While considerable research has focused on using either L-band or P-band SAR (Synthetic Aperture Radar) on their own for forest biomass retrieval, the use of the two bands simultaneously to improve forest biomass retrieval remains less explored. In this paper, we make use of L- and P-band airborne SAR and in situ data measured in the field together with laser scanning data acquired over one hemi-boreal (Remningstorp) and one boreal (Krycklan) forest study area in Sweden. We fit statistical models to different combinations of topographic-corrected SAR backscatter and forest heights estimated from PolInSAR for the biomass estimation, and evaluate retrieval performance in terms of R^2 and using 10-fold cross-validation. The study shows that specific combinations of radar observables from L- and P-band lead to biomass predictions that are more accurate in comparison with single-band retrievals. The correlations and accuracies between the combinations of SAR features and aboveground biomass are consistent across the two study areas, whereas the retrieval performance varied for individual bands. P-band-based retrievals were more accurate than L-band for the hemi-boreal Remningstorp site and less accurate than L-band for the boreal Krycklan site. The aboveground biomass levels as well as the ground topography differ between the two sites. The results suggest that P-band is more sensitive to higher biomass and L-band to lower biomass forests. The forest height from PolInSAR improved the results at L-band in the higher biomass substantially, whereas no improvement was observed at P-band in both study areas. These results are relevant in the context of combining information over boreal forests from future low-frequency SAR missions such as the European Space Agency (ESA) BIOMASS mission, which will operate at P-band, and future L-band missions planned by several space agencies.

Keywords: P-band synthetic aperture radar (SAR); L-band SAR; aboveground biomass estimation; boreal forest; forestry

1. Introduction

Forests are relevant as natural carbon storage in the global carbon cycle and thus, play an important role for climate change mitigation [1–3]. Information on forest biomass including its spatial distribution and change over time is essential in this respect as carbon content is related to forest biomass [4]. In 2013, the European Space Agency (ESA) selected a new satellite mission called BIOMASS who's main objective is to provide systematic and spatially-explicit estimates of forest height, biomass, and biomass change at global scale. The estimates are expected to help improve our understanding and quantification of forest carbon emissions and sinks, while reducing uncertainties in the global carbon cycle [5,6]. After launch, expected around 2021, the BIOMASS mission will use for the first time a space borne P-band synthetic aperture radar (SAR) to retrieve forest height and biomass estimates with global coverage of tropical and partial coverage of boreal forests. This band was selected specifically because of the good sensitivity of P-band backscatter to forest biomass in different biomes and high temporal coherence which supports complementary forest height retrieval using PolInSAR techniques [6–14].

In parallel there has been continuous work on forest bio-physical parameter retrieval using L-, C- and X-band SAR wavelengths [15–20]. In general this research has shown that—based on current algorithms and measurement systems—long wavelengths like L- and P-band are more sensitive to forest biomass than X- and C-band systems especially when considering radar backscatter signals [7,14–18,21]. This is attributed to the higher penetration capabilities of longer wavelengths which result in better sensitivity of the backscattering coefficient to forest biomass. The good sensitivity of the backscattered signal at L-band to aboveground biomass levels up to 100 t ha^{-1} and 150 t ha^{-1} is well documented [15,16,22–24], whereas for C-band backscatter appears to saturate at lower levels between 20 t ha^{-1} and 50 t ha^{-1} [7,16,21,25]. It is worth noting that newly developed algorithms to retrieve forest biomass using C-band at scales of a few kilometers can extend this range [26].

In addition to the ESA BIOMASS mission, future L-band SAR missions are being prepared by several agencies. These include NISAR (NASA and ISRO), SAOCOM (CONAE) and other missions currently in feasibility studies such as Tandem-L (DLR) and the next generation of ALOS for an L-band SAR mission (JAXA). Several of these missions also have as an objective to map forest aboveground biomass and forest heights [27,28] and overlap in time with BIOMASS. This opens up the possibility of combining spatially coincident measurements over forested areas from BIOMASS with corresponding measurements from L-band satellite missions to possibly enhance forest biomass retrievals and extend these in space and time. The potential of combining different radar bands for forest biomass estimation has been recognized in the past and motivated several studies [12,16,18,19,29]. Other studies suggested also an improvement of the biomass estimation by combining L-band with optical data and machine learning algorithms [30–32]. However, for some biomes such as boreal forests and Savannah woodlands only marginal improvements were observed combining L-band SAR with other frequencies [18,29,33]. This was attributed to the fact that the saturation limit for L-band SAR was not exceeded for the investigated study areas [18,29].

In addition to measuring the intensity of the radar backscatter, several of the new low-frequency SAR satellite missions are designed to support polarimetric SAR interferometry using repeat-pass (BIOMASS, NISAR, SAOCOM) or single-pass (Tandem-L) acquisitions [5,28]. This enables the retrieval of vegetation height using PolInSAR techniques [5,6,28,34,35] and this additional information can be used to support biomass estimation [36].

In this study we focus for the first time on combining both radar backscatter and vegetation height information estimated from PolInSAR at L- and P-band for boreal forests. The data analyzed in our study was used in the past, where limitations were observed in the individual utilization of L- and P-band for biomass estimation like limited sensibility of the signal to biomass (e.g., due to signal saturation), different soil moisture levels and topography [9,10,37]. The combination of different frequencies (like optical and SAR data) was used in different studies in order to overcome saturation limits [31,32,38,39]. However, it can be argued that optical data is not optimal for biomass estimation, whereas L- and P-band are assumed to have highest potential for biomass estimation [7,14–18,21]. Therefore, we assess in our study the potential to overcome limitations in both bands used in isolation by combining the information from P- and L-band in the same study areas. The aim of the study is to evaluate and quantify improvements in forest biomass retrieval using both frequencies and compare these with what can be achieved using only one of the frequencies in isolation (corresponding to a particular P- or L-band SAR mission). To our best knowledge, it is the first time that this was assessed in boreal forests and it can be argued that this information is of significance for future SAR missions using L- and P-band. The total forest biomass range addressed is 0 t ha^{-1} to 300 t ha^{-1} which is representative of full biomass range encountered in hemi-boreal and boreal forests.

2. Material

2.1. SAR Data

This study makes use of airborne SAR data together with coincident ground measurements collected during the ESA BioSAR-1 and -2 campaigns (see final reports of the campaign for full details [40,41]). The campaigns were conducted in March to May 2007 and October 2008 respectively over two different study areas located in Sweden: Remningstorp and Krycklan (Figure 1).

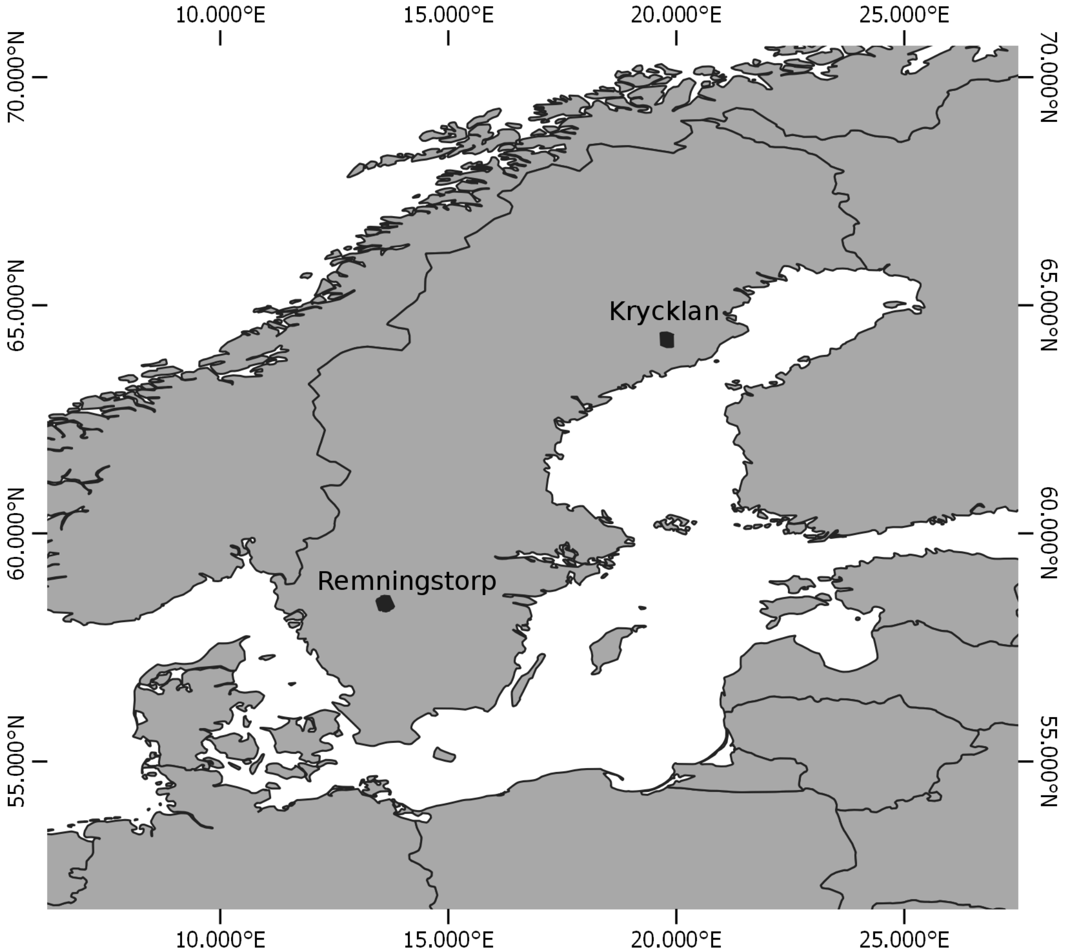

Figure 1. Location of the Remningstorp and Krycklan study areas in Sweden.

The E-SAR airborne system from the German Aerospace Center (DLR) was used to collect P- and L-band fully-polarimetric SAR imagery over both sites [40,41]. For P-band the center frequency f_c was 350 MHz (λ = 85.7 cm) and 1300 MHz (λ = 20 cm) for L-band. The airborne acquisitions covered about 20 km^2 in Remningstorp and 30 km^2 in Krycklan. Acquisitions which were suitable for PolInSAR height retrieval were used in this study. Across-track baselines of 8 m, 16 m, 24 m, 32 m and 40 m for P-band and 6 m, 12 m, 18 m, 24 m and 30 m for L-band were used in the BioSAR-2 campaign. In addition, PolInSAR data were acquired with two different flight heading angles with respect to north in Krycklan (Table 1) [41]. The soil moisture content was substantially higher on 9 March 2007 compared to the other acquisition dates in Remningstorp [10].

Table 1. Overview of used SAR acquisitions (after [40,41]; θ_i means incidence angle).

Campaign	Site	Dates	Band	θ_i (°)	Heading (°)	Resolution in Range/ Azimuth (m)	Across-Track Baseline (m)
BioSAR-2	Krycklan	14 October 2008	P-band	25–55	313	2.1/1.6	8–40
BioSAR-2	Krycklan	14 October 2008	P-band	25–55	133	2.1/1.6	8–40
BioSAR-2	Krycklan	15 October 2008	L-band	25–55	313	2.1/1.2	6–30
BioSAR-2	Krycklan	15 October 2008	L-band	25–55	133	2.1/1.2	6–30
BioSAR-1	Remningstorp	9 March 2007	P-band	25–55	200	2.1/1.6	10 & 80
BioSAR-1	Remningstorp	2 April 2007	P-band	25–55	200	2.1/1.6	30, 40, 50
BioSAR-1	Remningstorp	2 May 2007	P-band	25–55	200	2.1/1.6	20, 60, 70
BioSAR-1	Remningstorp	9 March 2007	L-band	25–55	200	2.1/1.2	8
BioSAR-1	Remningstorp	2 April 2007	L-band	25–55	200	2.1/1.2	8
BioSAR-1	Remningstorp	2 May 2007	L-band	25–55	200	2.1/1.2	8

2.2. Other Data Sets

The Remningstorp study area is a hemi-boreal forest with Norway spruce, Scots pine and birch as dominating tree species [10], whereas the Krycklan site further north is a boreal forest with dominant species limited to Norway spruce and Scots pine only [9]. For both sites airborne LiDAR data were acquired with the helicopter TopEye system covering the whole study areas [40,41]. The average measurement density was 30 pulses per m^2 in Remningstorp and 5 pulses per m^2 for Krycklan. Digital elevation (DEM) and canopy height models (CHM), which were extracted as maximum height in a grid cell of 0.5 m, were provided. The Remningstorp area is generally flat with elevations ranging from 120 m to 145 m above sea level [10]. The Krycklan area has a more pronounced topography with height variations of 100 m to 400 m above sea level [37].

Reference forest biomass data were derived based on field measurements in both sites. In total, 849 circular plots with a radius of 10 m were distributed systematically with a spacing of 40 m. For each plot the diameters at breast height (dbh) for trees with a dbh larger than 5 cm were measured, the tree species recorded and tree height measured for a subsample of the trees [10]. Stem volume was estimated with a stratum specific regression of multiple LiDAR metrics and tree measurements, which was further applied to all LiDAR raster cells [10]. These estimations were used to sample 58 homogeneous stands in Remningstorp with stand sizes between 0.5 ha and 9.4 ha and an average size of 2 ha [10,40]. Aerial photography supported the stratification and the definition of the stands [10]. The stem volume was converted to aboveground biomass by applying a biomass expansion factor, which was estimated on data collected in 10 independent 80 m by 80 m and 7 independent 50 m by 20 m sample plots [10,40]. Stands with dominating young forests were considered separately [10]. The 58 stands in Remningstorp had an average aboveground biomass of 129 t ha^{-1} with a range from 11 t ha^{-1} to 287 t ha^{-1} (Table 2). The average error in biomass is estimated to be 25 t ha^{-1} based on the independent sample plots [9,10].

Table 2. Summary of aboveground biomass values (in t ha^{-1}) of the forest stands.

Site	Mean	Standard Deviation	Minimum	Maximum	n
Krycklan	99.1	38.6	27.5	182.5	27
Remningstorp	129.0	54.0	10.5	287.3	58

For the Krycklan site a protocol was used with systematically distributed field plots. They were distributed in order to sample ten plots per forest stand and dbh measurements starting at trees with 4 cm dbh. Again, tree height was measured for a sample of trees and the height of trees without height measurements was determined by dbh to tree height relationships and the biomass estimated with species specific allometric relations [37]. In contrast to Remningstorp where biomass estimation was supported by LiDAR and aerial photography, the biomass was estimated solely with in situ data. Out of the 31 stands sampled, 27 of them were fully covered by the radar acquisitions and used for this study. The stand biomass values ranged from 28 t ha^{-1} to 183 t ha^{-1} with a mean of 99 t ha^{-1} (Table 2) [37,41].

3. Methods

3.1. SAR Backscatter Processing

The backscatter coefficient γ^0 was calculated for both campaigns and radiometrically calibrated from the complex SAR datasets in two steps, where first γ^0 was calculated at flat terrain ($\gamma_f^0 = \frac{\sigma^0}{\cos(\theta_i)}$, where σ^0 is the normalized radar cross section, θ_i is the incidence angle which is the angle between the line of sight and the vertical, and γ_f^0 represented the backscatter on flat terrain) and second corrected for topographic slopes. Topography generally alters the backscatter for similar land cover types and biomass levels and topographic correction is an active area of research [8,42–45]. A first step in topographic slope correction was to calculate topographic slope α_s and the aspect angle ϕ_s with respect to true north using the available LiDAR digital terrain models for each site and Horn's method [46]. The backscatter on (real) tilted terrain (γ^0) was then computed by following the approach of [47], where it is suggested that the terrain can be described as an opaque volume and the scatterer density per volume unit is constant. Following this method the terrain corrected backscatter coefficient γ^0 was given by

$$\gamma^0 = \gamma_f^0 \frac{\tan(90^\circ - \theta_i + \alpha_{rg})}{\tan(90^\circ - \theta_i)} \tag{1}$$

where the correction factor represents the ratio of the observed volume on a tilted terrain with respect to the volume which would have been illuminated in case of a flat terrain [42,47]. The tilt of the terrain was expressed by the slope steepness angle in range α_{rg}. This was calculated by first estimating the slope direction with respect to the range direction angle ϕ_{rg} through

$$\phi_{rg} = \phi_i - \phi_s \tag{2}$$

where ϕ_s is the topographic aspect angle with respect to true north and ϕ_i is the angle between the line of sight of the radar acquisition and true north in a horizontal plane [42]. Second, the slope steepness in range α_{rg} was calculated using the slope direction with respect to range direction ϕ_{rg} and the topographic slope angle of the terrain α_s [42]

$$\alpha_{rg} = \arctan(\tan(\alpha_s)\cos(\phi_{rg})) \tag{3}$$

We evaluated the quality of the topographic correction by following procedures suggested by [42,48], which involved the comparison of backscatter values from different acquisition headings. For Krycklan anti-parallel headings were used (313° and 133°), providing an ideal setting to test the performance of the corrections and both covering the full study area with the full range of topography in the study area. The corrected γ^0 values from (1) of both bands within the forest stands of Krycklan were extracted and the values from the acquisitions with different heading directions were compared. The values of the respective band and polarization resulted in high coefficients of determination (R^2 = 0.6 to 0.8) and small root mean squared differences (γ^0_{Diff} = -0.6 dB to -0.25 dB). These results indicated that the topographic correction used was sufficient in the forest areas of Krycklan [42,48]. As mentioned above, the Remningstorp area is relatively flat and thus, we assumed that the topographic correction was also sufficient for this area. It is worth noting that remaining differences can be attributed to speckle noise, geometrical and registration errors as well as topographical effects [48].

Look-up tables were provided in addition to the SAR acquisitions in order to determine each range and azimuth position to a geographic coordinate. These look-up tables were used to geocode the SAR backscatter images at L- and P-band in HH, HV, VH and VV polarization.

3.2. PolInSAR Processing

Forest heights have been estimated frequently with PolInSAR from L- and P-band SAR in different biomes [6,34,35,37,49–51]. The Random Volume over Ground (RVoG) model was used to retrieve the forest height from the L- and P-band full-polarimetric acquisitions in this study. This frequently used model is a two-layer-model consisting of a volume layer with randomly oriented scatterers over an impenetrable ground layer [34,49,50]. An exponential distribution is widely assumed to describe backscattering distribution of the volume layer [34,51–53]. The L- and P-band data were used separately to estimate the complex coherences as the cross correlation of two interferometric acquisitions and to retrieve forest height. The forest height was derived for each acquisition date separately. It can be assumed that the heights from different acquisition dates were highly correlated [40]. The combination of different dates was not possible in Krycklan. Therefore, the different dates were not combined in Remningstorp in order to avoid mixing baseline and temporal information as well as to sustain higher comparability with the results in Krycklan.

This RVoG model inversion was used to estimate vegetation height from the two bands with different baselines. Areas with a low coherence ($|\gamma| < 0.3$) were masked out in order to avoid erroneous vegetation height retrieval. The different vegetation height results based on various baselines were combined for the bands separately. The masked areas were filled with additional vegetation height estimates from acquisitions with a baseline where the coherence was higher then the coherence threshold. In areas where multiple valid vegetation height estimates were obtained, the vegetation height value was selected on basis of interferometric height accuracy as a function of standard deviation of the phase and the vertical wavenumber in order to achieve best possible inversion results [51,54]. Look-up tables were used again to geocode the vegetation height retrieval information, following a similar approach to backscatter data preprocessing.

3.3. Statistical Models for Forest Aboveground Biomass Estimation

As mentioned above, the data we used were content of a few previous studies. Therefore, the aboveground biomass estimation models based on SAR features were built on the findings of these studies. First, it was found that HV backscatter at L- and P-band had highest sensitivity compared to other polarizations over the full aboveground biomass range in Remningstorp (11 t ha^{-1} to 287 t ha^{-1}) [9,10]. In contrast, poor correlations between any single polarization at P-band and biomass were found in Krycklan with a smaller biomass range (28 t ha^{-1} to 183 t ha^{-1}) [37]. This was based on the low sensitivity of P-band to low biomass values, but also the topography in Krycklan [9,37]. However, the difference (or ratio) of HH and VV backscatter was suggested to overcome these limitations due to fact that this is sensitive to double bounce, which is based on ground and stem interactions related to stem biomass [29,37]. Further, it can be argued that topographic effects are similar in HH and VV polarization and thus, the ratio would reduce topographic effects [9]. In addition, forest height estimated via PolInSAR techniques resulted also in high correlations with biomass [37]. Consequently, we used models based on these previous findings and combined the two bands in the aboveground biomass estimation models as described in more detail below.

The mean backscatter of the topographic corrected γ^0 for the individual forest stands was extracted for every polarization and band in both study areas. In total, we defined 10 different statistical models which were used to link forest biomass to radar observables at L- and P-band. The first regression model B_1 was defined by

$$\log_{10} \mathrm{AGB}_{B_1} = a + b \cdot \gamma^0_{\mathrm{HV}}[\mathrm{dB}] \tag{4}$$

where AGB is the aboveground biomass expressed in tons per hectare (t ha^{-1}), a and b are the model parameters and B_i indicates the model index. It makes use of the log-relationship model between HV-polarized backscatter coefficient γ^0_{HV} in dB and aboveground biomass that has been extensively studied using L- and P-band SAR data over boreal and temperate forests [6,9,10,22,55,56]. The second model expanded the log-relationship model to include the ratio of HH and VV backscatter

$$\log_{10} \mathrm{AGB}_{B_2} = a + b \cdot \gamma^0_{\mathrm{HV}}[\mathrm{dB}] + c \cdot (\gamma^0_{\mathrm{HH}}[\mathrm{dB}] - \gamma^0_{\mathrm{VV}}[\mathrm{dB}]) \tag{5}$$

with γ^0_{HH} and γ^0_{VV} representing the backscatter at HH and VV polarization respectively and c representing a model parameter. The co-polarized ratio had been used by [9] for forest biomass retrieval as a complement to HV backscatter information as it reduces effects from the ground (e.g., moisture and topographic effects) as well for its sensitivity to stem biomass via double bounce scattering from ground and stem interaction.

The third model combined HV polarized backscatter at L- and P-band in a log-relationship model using multiple linear regression

$$\log_{10} \mathrm{AGB}_{B_3} = a + b \cdot \gamma^0_{\mathrm{HV}}[\text{L-band;dB}] + c \cdot \gamma^0_{\mathrm{HV}}[\text{P-band;dB}] \tag{6}$$

In a similar fashion as B_2, we used for the fourth model a linear combination of radar observables from both frequencies with the HV backscatter at L-band and the ratio of HH/VV backscatter at P-band yielding

$$\log_{10} \mathrm{AGB}_{B_4} = a + b \cdot \gamma^0_{\mathrm{HV}}[\text{L-band;dB}] + c \cdot (\gamma^0_{\mathrm{HH}}[\text{P-band;dB}] - \gamma^0_{\mathrm{VV}}[\text{P-band;dB}]) \tag{7}$$

The ratio was used because of the reduction of ground effects and the sensitivity to the stem biomass via double bounce scattering from ground/stem interactions [9,37]. Reference [57] found that the P-band penetrated deeper into the forest and was more affected by ground contributions than the L-band backscatter. Thus, it was assumed that the P-band backscatter HH/VV ratio had more potential to reduce the nuisance effects from the ground and to include sensitivity to stem biomass via double bounce effects compared to L-band. We calculated and extracted also the co-polarized phase difference ϕ_{HHVV} for the forest stands in order to verify the relevance of double bounce scattering at L- and P-band [58,59].

Having defined models based on intensity information only, we defined statistical regression models that include forest height information derived from PolInSAR as one of the observables. Linear models have been studied and shown to be useful to estimate aboveground biomass with heights from interferometric radar [60–62] and thus, we first defined a simple linear function of the height such that

$$\mathrm{AGB}_{B_5} = a + b \cdot h_{\mathrm{V}} \tag{8}$$

where h_{V} represents the PolInSAR vegetation height. An additional model used in the literature was based on a power law for the height [60,61,63] yielding the next model as

$$\mathrm{AGB}_{B_6} = a \cdot h_{\mathrm{V}}^b \tag{9}$$

Combining vegetation height estimated from PolInSAR with backscatter information, we expanded the log-relationship model for HV backscatter γ^0_{HV} adding vegetation height h_{V} as an additional variable yielding

$$\log_{10} \mathrm{AGB}_{B_7} = a + b \cdot \gamma^0_{\mathrm{HV}}[\mathrm{dB}] + c \cdot \log_{10} h_{\mathrm{V}} \tag{10}$$

As an extension we combined HV backscatter and HH/VV ratio in combination with PolInSAR vegetation height h_{V} such that

$$\log_{10} \mathrm{AGB}_{B_8} = a + b \cdot \gamma^0_{\mathrm{HV}}[\mathrm{dB}] + c \cdot (\gamma^0_{\mathrm{HH}}[\mathrm{dB}] - \gamma^0_{\mathrm{VV}}[\mathrm{dB}]) + d \cdot \log_{10} h_{\mathrm{V}} \tag{11}$$

Reference [37] suggested substantially higher correlations of aboveground biomass and vegetation height estimated from L-band PolInSAR compared to P-band. This was mainly based on the fact that the ground contribution was much larger than the forest canopy contribution at P-band compared to L-band [37]. Consequently, only the L-band height was used in our study in the combined biomass estimation. The co-polarized ratio was considered significant in the aboveground biomass estimation [9] and as mentioned above was assumed to have more potential for the biomass estimation at P-band than at L-band. Thus, this ratio was also used in the combined models. A saturation of backscatter at L-band for aboveground biomass levels around 100 t ha^{-1} to 150 t ha^{-1} was suggested in the past [15,16,23,24]. The aboveground biomass of forest stands in Remningstorp exceeded this biomass and thus, the P-band HV backscatter was used to estimate the aboveground biomass

$$\begin{aligned}\log_{10}\mathrm{AGB}_{B_9} = a + b\cdot\gamma^0_{\mathrm{HV}}[\text{P-band;dB}] + c\cdot(\gamma^0_{\mathrm{HH}}[\text{P-band;dB}] - \gamma^0_{\mathrm{VV}}[\text{P-band;dB}]) \\ + d\cdot\log_{10} h_{\mathrm{V}}[\text{L-band}]\end{aligned} \tag{12}$$

In addition, an aboveground biomass estimation model was also used with L-band HV backscatter and P-band HH/VV ratio similar to B_4 with the extension of L-band PolInSAR vegetation height

$$\begin{aligned}\log_{10}\mathrm{AGB}_{B_{10}} = a + b\cdot\gamma^0_{\mathrm{HV}}[\text{L-band;dB}] + c\cdot(\gamma^0_{\mathrm{HH}}[\text{P-band;dB}] - \gamma^0_{\mathrm{VV}}[\text{P-band;dB}]) \\ + d\cdot\log_{10} h_{\mathrm{V}}[\text{L-band}]\end{aligned} \tag{13}$$

All model parameters were estimated with least square regression for all models [64,65]. The individual models were applied to the whole coverage of L- and P-band radar acquisitions in order to create biomass maps for illustrative purposes. The acquisition dates were considered separately. A forest/non-forest classification, which was described in [66], was used to mask out non-forest areas for visual purposes. The biomass in logarithmic scale was transformed to linear scale. The transformation of logarithmic data produces a bias. Assuming that the residuals of the regression were normally distributed, this bias could be accounted for by a correction factor calculated as $10^{\mathrm{MSE}/2}$, where MSE is the mean square error [67]. The correction factor for the logarithmic transformation was on average 1.01 with 0.01 standard deviation over all models. Therefore, the logarithmic transformation error was assumed to be negligible in this case.

3.4. Validation of Aboveground Biomass Estimation

The coefficient of determination R^2 of each biomass estimation model was calculated with

$$R^2 = 1 - \frac{\sum_{i=1}^{n}(y_i - \hat{y}_i)^2}{\sum_{i=1}^{n}(y_i - \bar{y})^2} \tag{14}$$

where y_i means actual value of i, $\hat{y}_i$ means modeled value of i and $\bar{y}$ is the mean of the actual values. The different coefficients of determination for the various biomass estimation models were compared. The t-statistics and corresponding p-values for each coefficient (feature) in the linear models were calculated in addition to the performance metrics of the different regression models. The p-value provided information about the significance of a coefficient, where a p-value below the significance level α of 0.05 resulted in a rejected null hypothesis meaning that the coefficient was considered significant [64,65]. All available samples in the respective study area were used for these metrics.

An explicit validation data set was not available and thus, a k-fold cross-validation was applied in order to estimate the goodness of the models [68,69]. The subsamples were selected randomly and k was set to 10 for all biomass estimation models. The root mean square error (RMSE) was then calculated for each biomass model in all folds of the 10-fold cross-validation

$$\text{RMSE} = \sqrt{\frac{1}{n}\sum_{i=1}^{n}(y_i - \hat{y}_i)^2} \;\&\; \text{RMSE (in \%)} = \frac{\text{RMSE}}{\bar{y}} \times 100 \tag{15}$$

The RMSE values of the subsamples were finally averaged and their standard deviation was calculated to assess overall variability in the model fitting. A *t*-test with the error values of the different models was performed and corresponding *p*-values were calculated in order to test if the RMSE difference of individual models was significant. In addition, the corrected Akaike information criterion (AICc) was calculated for all models. This metric provides a further quality measure of the models and is used in model selection processes [70]. Therefore, the combination of R^2, RMSE and AICc could be used to select the best model for the biomass estimation in the hemi-boreal and boreal forest.

4. Results

4.1. Aboveground Biomass Estimation with SAR Backscatter

4.1.1. Remningstorp

The results for the regression models applied to each test site are summarised in Table 3. P-band backscatter showed a higher correlation with aboveground biomass compared to L-band in the forests of Remningstorp (Figure 2). The coefficient of determination of the log-relationship model B_1 between HV backscatter and biomass was 0.68 for L-band and 0.73 for P-band on 2 May 2007 (Table 3). The addition of the ratio between HH and VV (B_2) increased the R^2 value negligible for L-band, whereas for P-band, an increase to 0.83 was achieved. The lower AICc value for B_2 compared to B_1 at P-band confirmed the improvement. A *p*-value of <0.001 for the HV backscatter at L-band as well as for the HV backscatter and co-polarized ratio at P-band suggested significance, which was calculated with the *t*-test. The R^2 values were almost similar at P-band for the different dates (with different soil moisture) of acquisition with 0.74 for B_1 (B_2 = 0.83) on 09 March, 2007 and 0.72 for B_1 (B_2 = 0.83) on 2 April 2007. In contrast, the coefficients of determination at L-band differed on the different acquisition dates with 0.41 for B_1 (B_2 = 0.5) on 09 March, 2007 and 0.63 for B_1 (B_2 = 0.65) on 31 March 2007. However, main objective of this study was to assess the potential of the L- and P-band combination for aboveground biomass retrieval and thus, the best case scenario based on the acquisitions on 02 May, 2007 is further presented.

The aboveground biomass estimation with P-band HV backscatter alone (B_1) achieved an RMSE of 37.4 t ha^{-1} (25.9%; Table 3), whereas the combination of HV backscatter and ratio of HH and VV (B_2) achieved an RMSE of 31.8 t ha^{-1} (22%). For L-band, the RMSE of aboveground biomass estimation was 43.6 t ha^{-1} (30.2%) using the HV backscatter and HH/VV ratio (B_2). It is worth noting that the combination of HV backscatter and HH/VV backscatter ratio did not only improve the RMSE, but also the standard deviation of the RMSE was decreased (Table 3).

The combination of L- and P-band HV backscatter in the B_3 model improved the R^2 to 0.78 compared to the HV backscatter from the bands individually. The L- and P-band HV backscatter resulted in a *p*-value of <0.001 in this linear regression model and thus were considered significant (Table 4). The RMSE of this multiple linear relationship was 36.5 t ha^{-1} (25.3%; Table 3). The combination of L-band HV backscatter and P-band HH/VV ratio (B_4) improved the R^2 to 0.86 and achieved the highest coefficient of determination of all analyzed regressions based on backscatter information. The AICc value of -95.3 was also lowest in using the intensities only. The aboveground biomass estimation model B_4 resulted in a cross-validated RMSE of 32.9 t ha^{-1} (22.8%). This was significantly different compared to the L-band model, but not to the corresponding P-band model B_2. In addition, the standard deviation of RMSE was smallest in the combined aboveground biomass estimations (B_3 and B_4) compared to the bands in isolation (B_1 and B_2). L-band HV backscatter and P-band HH/VV ratio achieved a *p*-value of <0.001 and thus, both predictors were considered significant (Table 4).

Table 3. Coefficient of determination R^2, RMSE and AICc for different aboveground biomass estimation models (see Section 3.3 for the used predictors in each model). Each row corresponds to the same model applied to each frequency separately (first 7 columns) and then to both frequencies (last 4 columns). The standard deviation of the 10-fold cross-validated RMSE is provided (±) and n.a. means not applicable e.g., no corresponding dual-frequency version of the model. Significance of difference between single-band RMSE and corresponding combined RMSE (indicated in the same row of the table) is presented as * for a p-value < 0.05, ** <0.01 and *** <0.001; *n.s.* means not significant with significance level α of 0.05. Remningstorp results are based on acquisitions on 2 May 2007 and Kryckland results are based on 313° heading.

	Model	L-Band			P-Band			Model	L- and P-Band		
		R^2	RMSE (%)	AICc	R^2	RMSE (%)	AICc		R^2	RMSE (%)	AICc
Remningstorp	B_1	0.68	30.2 ± 10.5 *	−51.9	0.73	25.9 ± 8.3 $^{n.s.}$	−55.0	B_3	0.78	25.3 ± 7.1	−77.7
	B_2	0.69	29.5 ± 8.5 **	−48.5	0.83	22.0 ± 7.3 $^{n.s.}$	−67.2	B_4	0.86	22.8 ± 5.5	−95.3
	B_5	0.66	24.5 ± 9.4	−34.5	0.34	33.6 ± 8.8	−14.6	n.a.	n.a.	n.a.	n.a.
	B_6	0.67	24.2 ± 9.3	−30.9	0.36	32.7 ± 8.0	−9.3	n.a.	n.a.	n.a.	n.a.
	B_7	0.80	23.4 ± 9.0 $^{n.s.}$	−68.0	0.76	24.6 ± 7.5 *	−56.0	B_9	0.84	21.4 ± 7.4	−92.6
	B_8	0.80	24.2 ± 7.8 *	−65.6	0.83	21.8 ± 6.5 $^{n.s.}$	−73.1	B_{10}	0.86	20.8 ± 8.2	−108.6
Krycklan	B_1	0.83	17.4 ± 6.2 $^{n.s.}$	−50.7	0.25	29.5 ± 10.6 *	−13.0	B_3	0.83	18.6 ± 7.0	−47.9
	B_2	0.83	18.8 ± 8.4 $^{n.s.}$	−49.8	0.60	24.3 ± 9.3 *	−25.1	B_4	0.84	18.8 ± 7.2	−49.1
	B_5	0.61	24.3 ± 8.5	−32.5	0.30	31.7 ± 8.6	−13.3	n.a.	n.a.	n.a.	n.a.
	B_6	0.65	23.4 ± 8.1	−34.0	0.33	31.0 ± 8.5	−14.4	n.a.	n.a.	n.a.	n.a.
	B_7	0.84	17.7 ± 7.2 $^{n.s.}$	−48.9	0.55	21.5 ± 11.7 $^{n.s.}$	−25.7	B_9	0.75	20.6 ± 9.1	−34.2
	B_8	0.84	19.7 ± 10.5 $^{n.s.}$	−45.8	0.66	22.7 ± 13.0 *	−27.4	B_{10}	0.84	18.9 ± 7.1	−46.5

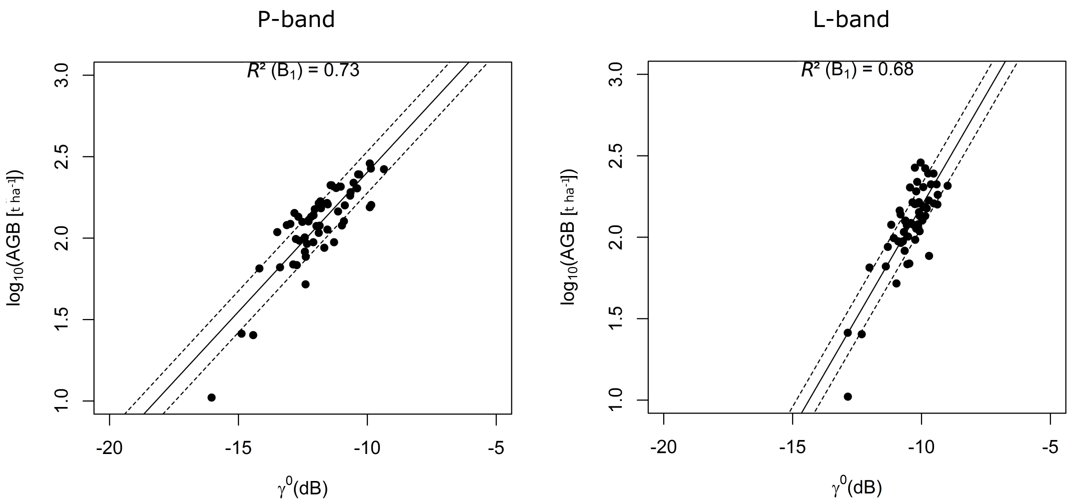

Figure 2. Log relationship between HV backscatter (γ^0 [dB]) and aboveground biomass of forest stands for P- (**left**) and L-band (**right**) in Remningstorp (dashed line is for the uncertainty of the intercept; 2 May 2007).

Table 4. Significance of coefficients (predictors) in the different aboveground biomass estimation models in Remningstorp/Krycklan (B_1 to B_{10}, see also Section 3.3 for a detailed description of the models and their coefficients, models with ^{LP} include both P- and L-band and * is for a p-value <0.05, ** <0.01 and *** <0.001; n.s. means not significant with significance level α of 0.05; *n.a.* means not applicable and this predictor was not used in the respective model; Remningstorp results are based on acquisitions on 2 May 2007 and Krycklan results are based on 313° heading).

Model	L-Band			P-Band		
	γ^0	γ^0_{HH}[dB] − γ^0_{VV}[dB]	h_V	γ^0	γ^0_{HH}[dB] − γ^0_{VV}[dB]	h_V
B_1	***/***	*n.a.*	*n.a.*	***/**	*n.a.*	*n.a.*
B_2	***/***	n.s./n.s.	*n.a.*	***/n.s.	***/***	*n.a.*

Table 4. *Cont.*

Model	L-Band			P-Band		
	γ^0	$\gamma^0_{\mathbf{HH}}[\mathbf{dB}] - \gamma^0_{\mathbf{VV}}[\mathbf{dB}]$	h_{V}	γ^0	$\gamma^0_{\mathbf{HH}}[\mathbf{dB}] - \gamma^0_{\mathbf{VV}}[\mathbf{dB}]$	h_{V}
B_3^{LP}	***/***	*n.a.*	*n.a.*	***/n.s.	*n.a.*	*n.a.*
B_4^{LP}	***/***	*n.a.*	*n.a.*	*n.a.*	***/n.s.	*n.a.*
B_5	*n.a.*	*n.a.*	***/***	*n.a.*	*n.a.*	***/**
B_7	***/***	*n.a.*	***/n.s.	***/***	*n.a.*	**/***
B_8	***/***	n.s./n.s.	***/n.s.	***/*	***/*	n.s./*
B_9^{LP}	*n.a.*	*n.a.*	*/***	***/n.s.	***/n.s.	*n.a.*
B_{10}^{LP}	***/***	*n.a.*	*/n.s.	*n.a.*	***/n.s.	*n.a.*

The comparison of co-polarized phase differences ϕ_{HHVV} revealed a higher phase difference for P-band ranging from -2 to -0.5 with an average of -1.32 compared to L-band with a range of -0.9 to -0.3 and an average of -0.52 (Figure 3). This confirmed that the penetration depth and double bounce contribution was higher at P-band compared to L-band resulting also in a higher difference of HH and VV backscattering.

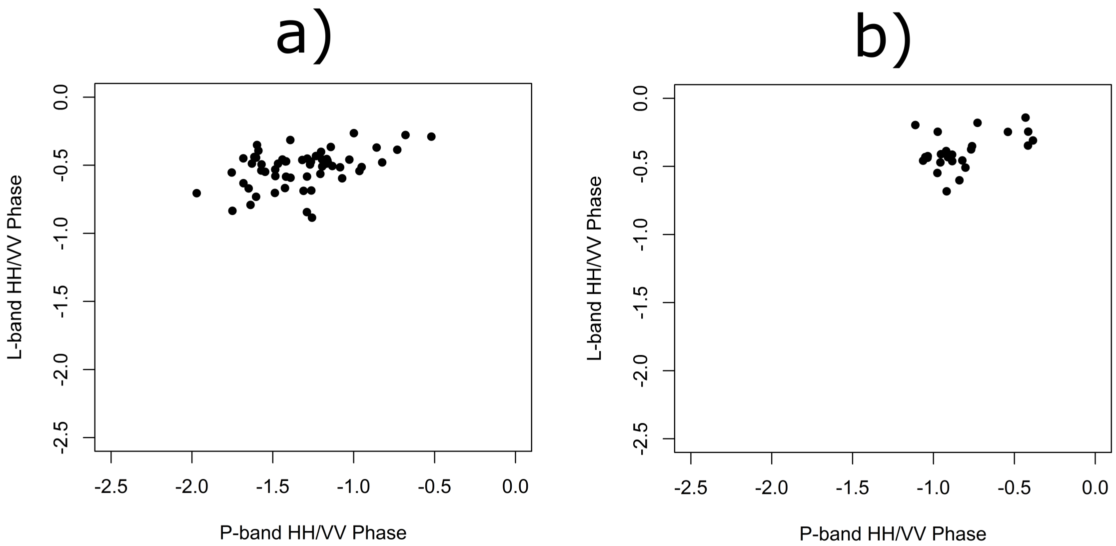

Figure 3. Comparison of co-polarized phase difference of P- and L-band in the forest stands in Remningstorp ((**a**) 2 May 2007) and Krycklan ((**b**) 313°).

4.1.2. Krycklan

The log-relationship model B_1 with P-band resulted in an R^2 of 0.25 in Krycklan (Figure 4). The utilization of the co-polarized backscatter ratio in biomass modeling (B_2) achieved a substantially higher R^2 value of 0.6 and a lower RMSE of 24.1 t ha^{-1} (24.3%) compared to backscatter only with an RMSE of 29.2 t ha^{-1} (29.5%; Table 3). The ratio resulted in a p-value of $<$0.001 and the HV backscatter achieved a p-value of 0.068 (Table 4).

In contrast to Remningstorp, L-band backscatter resulted in higher R^2 with aboveground biomass of 0.83 compared to P-band (B_1, Figure 4). Similar to Remningstorp, the co-polarized ratio at L-band was considered insignificant in the B_2 model (p-value of 0.826). Further, the AICc value was almost similar in the combination of HV backscatter and HH/VV ratio (B_2) at L-band compared to HV backscatter alone (B_1). The resulting models achieved RMSE values for the log-relationship model B_1 of 17.3 t ha^{-1} (17.4%) and 18.7 t ha^{-1} (18.8%) for B_2 (Table 3).

The L- and P-band combination resulted in an R^2 value of 0.84 (B_3), which was similar to the individual L-band results with 0.83 (Table 3). Consequently, no improvement in AICc was observed in the combination of P- and L-band HV backscatter (B_3). The L-band HV backscatter achieved a p-value of <0.001 in the biomass regression model B_4, whereas the P-band HH/VV ratio resulted in a p-value of 0.294. Therefore, the ratio could be considered insignificant assuming a significance level at 0.05. The combination of bands achieved similar accuracies and AICc values compared to the individual L-band retrieval, whereas the standard deviation of the RMSE was decreased in the combined B_4 model (Table 3).

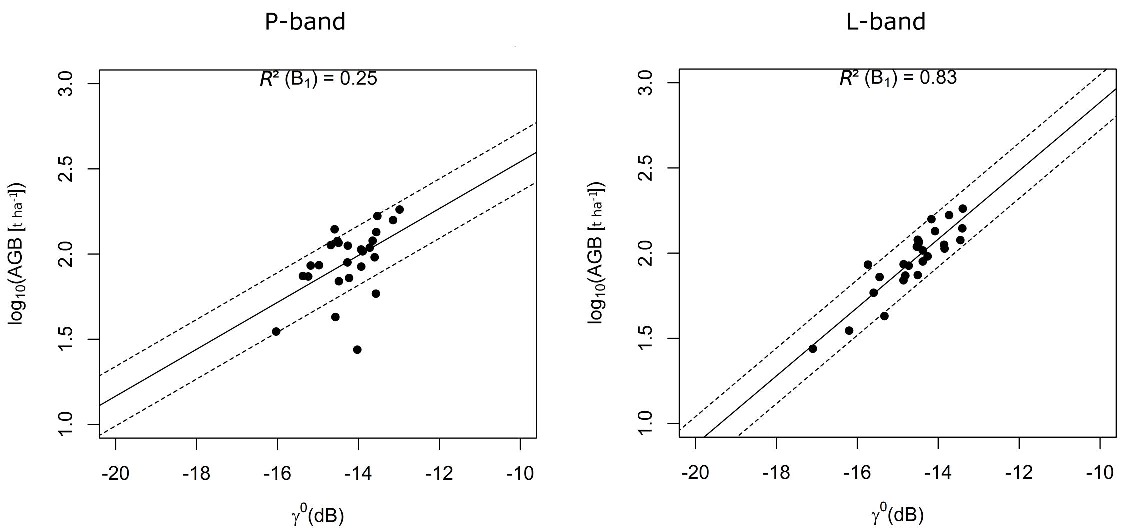

Figure 4. Log relationship between HV backscatter (γ^0 [dB]) and aboveground biomass of forest stands for P- (**left**) and L-band (**right**) in Krycklan (dashed line is for the uncertainty of the intercept; 313° heading).

The co-polarized phase difference ϕ_{HHVV} was similar to Remningstorp higher at P-band compared to L-band. The phase difference at P-band ranged from -1.1 to -0.4 with an average of -0.78, whereas it ranged from -0.7 to -0.14 with an average of -0.38 at L-band (Figure 3). This confirmed again that double bounce scattering was larger at P-band than at L-band.

4.2. Aboveground Biomass Estimation with PolInSAR Height and Combination with SAR Backscatter

4.2.1. Remningstorp

All PolInSAR heights based on the acquisitions from different dates were highly correlated ($R^2 \geq 0.9$) and differed by a root mean squared difference of $\leq$ 2m. Therefore, the correlations between the vegetation heights at different dates and aboveground biomass were similar, which confirms equivalent observations in [40]. Consequently, we focus in the following on the vegetation height results from 2 May 2007 corresponding to the backscatter analysis in Remningstorp.

The vegetation height estimated from P-band PolInSAR approach (B_5 and B_6) resulted in lower coefficients of determination compared to the aboveground biomass estimation with P-band backscatter. A coefficient of determination of 0.36 was achieved with the power model B_6 in the correlation of PolInSAR height and biomass. The linear model B_5 resulted in an R^2 of 0.34 (Figure 5). In contrast, the L-band PolInSAR height achieved higher R^2 values of 0.67 for the power B_6 and 0.66 for the linear model B_5 (Figure 5). The cross-validated RMSE at L-band was 35.4 t ha^{-1} (24.5%), whereas the RMSE of the aboveground biomass estimation with P-band PolInSAR height was 48.5 t ha^{-1} (33.6%; Table 3).

The aforementioned results showed the potential of aboveground biomass retrieval based on backscatter and PolInSAR vegetation height individually. However, both quantities were also combined (in models B_7 to B_{10}). The utilization of PolInSAR height and backscatter information at P-band resulted in no or small improvement of R^2 compared to backscatter information alone. The combination of backscatter and PolInSAR height information at P-band achieved an R^2 of 0.83 for

B_8 and 0.76 for B_7, whereas the R^2 for backscatter information alone was 0.83 (B_2) and 0.72 (B_1, Table 3). Consequently, the improvement of AICc was small. The PolInSAR height information was considered insignificant with a p-value of 0.515. In contrast, HV backscatter and ratio of HH and VV backscatter achieved a p-value of <0.001 and thus were considered significant. The L-band PolInSAR height as well as HV backscatter were considered significant in the biomass estimation (B_7, Table 4). An improvement of R^2 (0.8) and RMSE (23.4%) was achieved utilizing the PolInSAR height in combination with the backscatter in the model B_7 compared to utilizing the various information alone in the model B_1 (R^2 = 0.68; RMSE = 30.2%). The AICc value improved from −51.9 (B_1) to −68.0 (B_7).

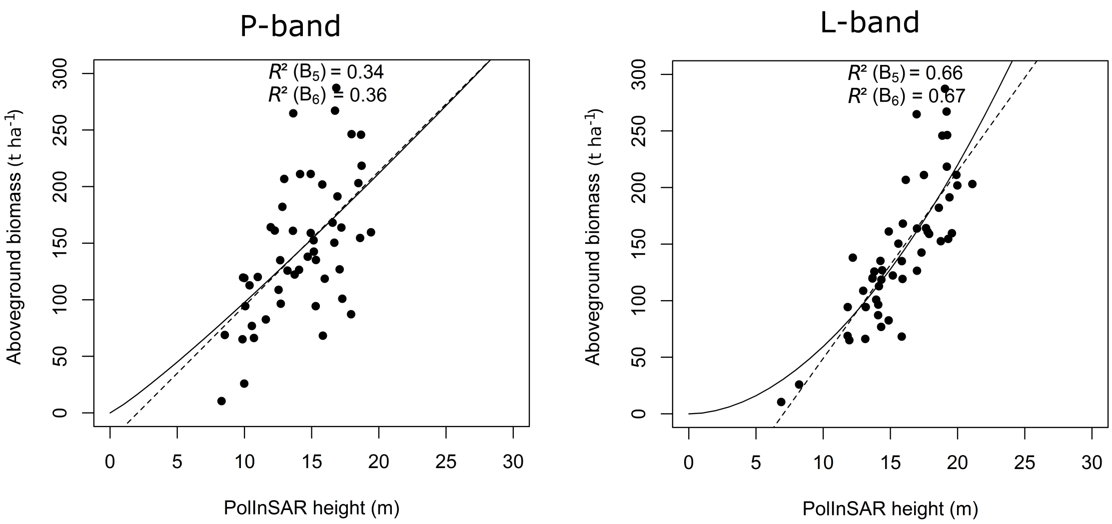

Figure 5. PolInSAR height and aboveground biomass regression based on P- (**left**) and L-band (**right**) in Remningstorp (Data acquired on 2 May 2007).

The L-band PolInSAR height and the backscatter at P-band were considered significant in biomass estimation with the individual bands. The combination of these features was also used to estimate the aboveground biomass in the hemi-boreal forest study area. The combination of P-band HV backscatter, P-band HH/VV ratio and L-band PolInSAR vegetation height (B_9) resulted in an R^2 of 0.84 and an RMSE of 31 t ha^{-1} (21.4%). All coefficients were considered significant with p-values of <0.001 for HV backscatter and HH/VV ratio and 0.019 for PolInSAR height. Similarly, all coefficients were considered significant when combining the L-band HV backscatter (<0.001), P-band HH/VV ratio (<0.001) and L-band PolInSAR height (0.047) in the B_{10} model. The B_{10} model resulted in an R^2 of 0.86, an RMSE of 30.1 t ha^{-1} (20.8%) and the lowest AICc value of −108.6 (Table 3). The average RMSE of the k-fold cross-validation was generally decreased in the combinations of the two bands resulting in significantly different RMSE compared to L-band B_8 model, whereas the standard deviation was similar or higher in the combination compared to the individual bands.

Aboveground biomass values from 0 to >300 t ha^{-1} were estimated in the hemi-boreal study area of Remningstorp. Large agricultural fields were identified in the south and north-west, whereas highest biomass values occurred in the center of the study area (Figure 6a). In general, the aboveground biomass estimation with L-band resulted in higher biomass values especially in the west and north of the study area compared to the estimation with P-band. The combined aboveground biomass estimation had a similar appearance like the aboveground biomass estimated with P-band alone (Figure 6a). Deviations from the 1:1 line in the comparison of estimated and actual biomass were smallest in the combination of backscatter and PolInSAR height compared to the backscatter-based retrievals of the individual bands (Figure 7).

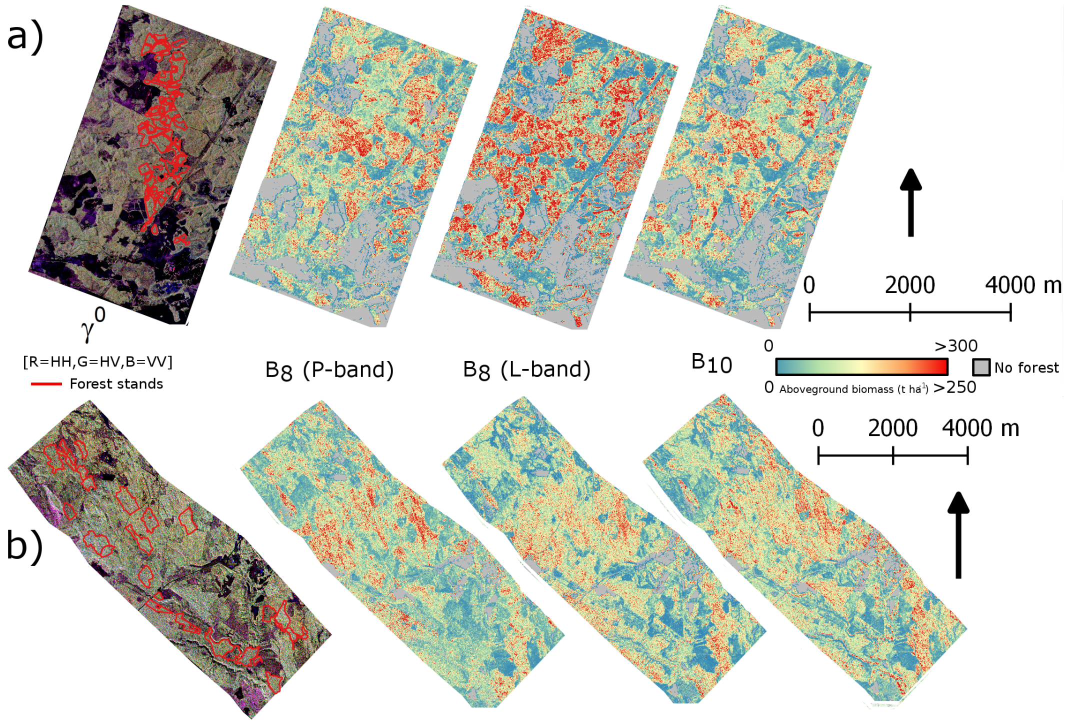

Figure 6. Spatial representation of L-band backscatter coefficient γ^0 with location of forest stands, aboveground biomass estimated with backscatter and PolInSAR height at P- and L-band (center) and biomass model combining the two bands (right) in Remningstorp (**a**) and Krycklan (**b**). Please note that the aboveground biomass of the stands ranged to 183 t ha^{-1} in Krycklan and 287 t ha^{-1} in Remningstorp and thus, estimations above these values may not be reliable.

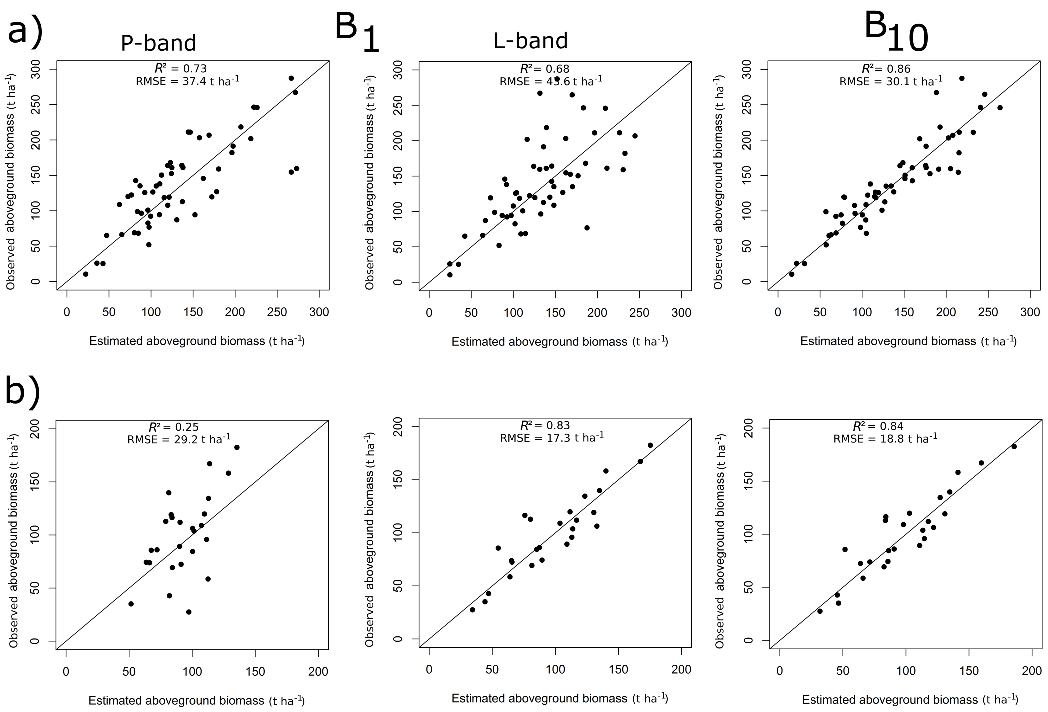

Figure 7. Estimated aboveground biomass using biomass models B_1 with P-band (**left**), B_1 with L-band (**center**) and B_{10} (**right**) compared to actual aboveground biomass in Remningstorp (**a**) and Krycklan (**b**; line corresponds to a 1:1 relationship).

4.2.2. Krycklan

The results of PolInSAR vegetation height for aboveground biomass estimation differed substantially between the bands in their coefficients of determination and accuracies similar to the backscatter results in Krycklan. The linear regression of aboveground biomass and L-band PolInSAR height (B_5) resulted in an R^2 of 0.61 and the power model (B_6) achieved an R^2 of 0.65 (Figure 8). The coefficient of determination in the linear regression of aboveground biomass and P-band PolInSAR height was 0.3 (B_5, Figure 8). In general, the coefficients of determination in the regression of aboveground biomass and PolInSAR heights were similar in both study areas. It is worth noting that the R^2 for the exponential models was calculated with (14). This may be inadequate for non-linear models and only appropriate for linear models [71]. However, the used power models were close to a linear model in both study areas. Thus, the calculated R^2 could be assumed appropriate also for these non-linear models. The aboveground biomass retrieval with L-band PolInSAR height achieved an RMSE of 24.1 t ha^{-1} (24.3%) and the P-band height achieved an RMSE of 31.4 t ha^{-1} (31.7%) with the linear B_5 model.

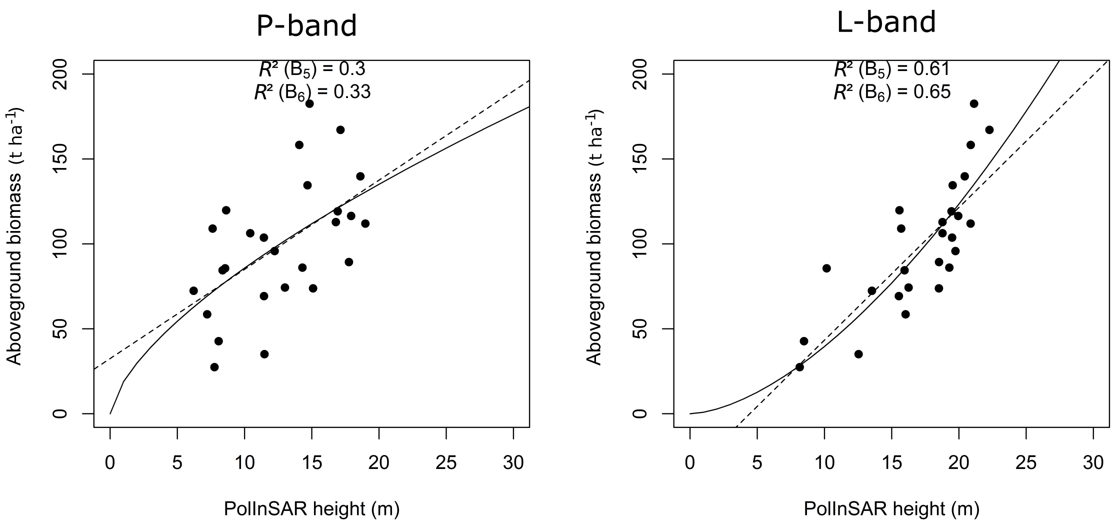

Figure 8. PolInSAR height and aboveground biomass regression based on P- (**left**) and L-band (**right**) in Krycklan.

As expected based on the results of backscatter information alone in Krycklan, the L-band achieved highest accuracies also in the combination of backscatter and PolInSAR height information (B_7) with an R^2 of 0.84 and an RMSE of 17.5 t ha^{-1} (17.7%) compared to P-band with an R^2 of 0.55 and an RMSE of 21.3 t ha^{-1} (21.5%; Table 3 and Figure 7 bottom). The ratio of HH and VV as well as the PolInSAR height did not contribute significantly to the aboveground biomass retrieval in L-band with p-values of 0.69 and 0.583, whereas the HV backscatter achieved a significant p-value of <0.001 (B_8, Table 4). In contrast, the HV backscatter, the ratio of HH and VV as well as the P-band vegetation height contributed significantly to the regression with aboveground biomass with p-values of 0.01, 0.033 and 0.029 at P-band (B_8).

Furthermore, the backscatter and PolInSAR height at P- and L-band were also combined for aboveground biomass estimation in the Krycklan study area (B_9 and B_{10}). The L-band backscatter was the only significant predictor in the aboveground biomass retrieval with a p-value of <0.001. The HH/VV backscatter ratio at P-band and L-band PolInSAR height achieved p-values of 0.44 and 0.47 (B_{10}, Table 4). The L-band backscatter in combination with P-band ratio and L-band PolInSAR height (B_{10}) resulted in a similar R^2 of 0.84 compared to L-band individually and an RMSE of 18.8 t ha^{-1} (18.9%). The lowest AICc value in Krycklan was achieved using the L-band HV backscatter alone (B_1), whereas the combination of L- and P-band did not decrease the AICc. The similar performance of biomass estimations with L-band alone or combined with other predictors was also visible in the deviations of the 1:1 line in the comparison of actual and estimated biomass since they did not differ substantially (Figure 7). The P-band backscatter, P-band ratio and L-band PolInSAR height (B_9) achieved a coefficient of determination of 0.75 with an RMSE of 20.4 t ha^{-1} (20.6%; Table 3), where the PolInSAR height was the only significant predictor (p-value of 0.001).

As expected, the estimated aboveground biomass values were generally lower in the boreal study area of Krycklan compared to the hemi-boreal forests of Remningstorp. The estimated aboveground biomass ranged from 0 t ha^{-1} to >250 t ha^{-1}. Highest aboveground biomass estimates were identified in the south-east. Lowest biomass values occurred in the south and in the north of the study area (Figure 6b). In contrast to Remningstorp, the combined aboveground biomass estimation had a similar appearance than the aboveground biomass estimated with L-band alone (Figure 6b).

5. Discussion

The biomass retrieval performance at L- and P-band when each band is used in isolation varied strongly from one site to the other. This could be based on the fact that the two sites differ in their ground topography, forest structure and biomass values, but were similar in their dominating tree species. However, effects of ground topography were corrected to a certain extent. The cross comparison of different heading angle flights suggested that topography was corrected sufficiently for the purpose of the study. Thus, the results indicate a different sensitivity of the two bands to certain biomass levels. It was observed that P-band performed better than L-band in the biomass estimation with B_1 and B_2 model in the Remningstorp site with higher R^2 values as well as lower RMSE and AICc. For the Kryklan site, however, the contrary was true and it was the L-band that provided higher R^2 values as well as lower RMSE and AICc. The better performance of L-band in Krycklan compared to P-band was also observed in a previous study [37]. It is worth noting, that [37] used a different backscatter coefficient normalization, not accounting for the local topography and thus, correlations and accuracies between SAR backscatter and biomass were improved in our study compared to the results from [37]. The stands of Remningstorp had a larger range of biomass of 11 t ha^{-1} to 287 t ha^{-1} compared to 28 t ha^{-1} to 183 t ha^{-1} in Krycklan. It could be argued that the saturation limit in the relationship of the backscatter at L-band to aboveground biomass was reached with this range of biomasses in Remningstorp. Machine learning algorithms and the combination of L-band with optical data were frequently used to overcome the saturation limit, whereas the potential of optical data for biomass estimation is also limited [30–32]. The P-band achieved generally higher correlations between backscatter and biomass in the forest with a larger biomass range compared to the L-band backscatter and thus, is assumed to have high potential to overcome the saturation limit. This is in line with observations in boreal forests of Alaska [55], forests of Maine [22] and as expected in the same study area using the same datasets [10], where all had a similar range of actual biomass of <100 t ha^{-1} to about 300 t ha^{-1}. The results of the different acquisition dates with different soil moisture conditions also suggest that P-band is less sensitive to moisture effects especially after applying the HH/VV ratio, which reduces these effects. In contrast, L-band seems more sensitive to moisture effects and thus results in different accuracies of aboveground biomass estimation. The different temporal stability of the two bands was previously observed using the same datasets [10].

The results of this study indicate that using combinations of radar observables from L- and P-band lead to retrievals that are more accurate with respect to the study area. This can be seen in the results for linear models combining γ^0_{HV} for L-band and P-band (B_3) and especially for model B_4 which uses γ^0_{HV} at L-band and the P-Band HH/VV co-polarized ratio. These models provided the best overall performance in the aboverground biomass estimation for both study areas and retrieval accuracy was at least as good as the best single-band results and in general better. This was confirmed by the lowest AICc value for biomass retrievals with backscatter only (B_4) compared to B_1 and B_2 in Remningstorp and similar AICc values for model B_4 and B_1 at L-band in Krycklan. Consequently, the combination is complementary due to the different sensitivity to biomass of the two bands.

The analysis of *p*-values confirmed that the ratio was more significant than the HV backscatter for aboveground biomass estimation with P-band data. Reference [9] suggested similarly high importance of the ratio due to the fact that moisture and topographic effects are similar in HH and VV polarizations and thus, could be removed in their ratio [9]. HH and VV backscatter differ mainly at double bounce effects like ground and stem interaction and thus, the ratio might be also sensitive to the stem biomass and consequently to the total forest biomass [9,29,37]. However, the co-polarized ratio should be combined with HV backscatter since this polarization has the highest sensitivity to biomass [6,9]. This is confirmed by the significance of HV backscatter expressed by the *p*-value in the linear regressions. Unlike in the case of the P-band, the co-polarized ratio were considered insignificant in the aboveground biomass estimation with L-band backscatter. This might be due to the fact that the L-band penetrates less into the forest having a stronger volume component from the canopy than P-band [57]. Consequently, the double bounce effects from ground and stem interaction as well as the removal of effects from the ground is limited in L-band, which is confirmed by the comparison of the phase differences of HH and VV polarization.

In terms of PolInSAR height, L-band heights showed a reasonable sensitivity to forest biomass with coefficients of determination R^2 generally above 0.6 for both sites, whereas P-band PolInSAR heights did not correlate well with biomass yielding higher errors and lower R^2 around 0.3. This is likely due to the high penetration of the P-band signal into the canopy resulting in a strong ground contribution and small canopy contribution [37]. A fundamental assumption of the applied PolInSAR retrieval is that there exists a polarization which contains no ground contribution. The assumption is likely violated at P-band, which is also confirmed through tomographic SAR (TomoSAR) analysis [57]. Any residual ground contribution in the volume-only coherence results in an overestimation of height [72]. Further, the frequently applied exponential distribution was assumed to model the vertical distribution of scatterers, where also other models could be used to improve the PolInSAR vegetation height retrieval with P-band [51]. In addition, Reference [37] suggested that the across-track baselines of BioSAR-2 campaign were relatively small resulting in low height sensitivity. Furthermore, the Krycklan study area was a hilly terrain with an elevation range of about 300 m and thus, it could be assumed that the topography was an influential factor on the accuracy. All this could result in erroneous vegetation heights (e.g., a vegetation height despite almost no biomass in Figure 5). This means that the height values might be inappropriate for forest biomass estimation. The correction of topography and a stratification of topography, biomass or land cover could increase the accuracy of aboveground biomass estimation with PolInSAR height [37,51].

In general, it was also observed that the retrieval accuracy using height only is lower than using intensity observables. However, it could be expected that the P-band PolInSAR height (and also the P-band backscatter) may be more appropriate in higher biomass forests. For instance, an improvement of aboveground biomass estimation in other studies in high biomass tropical forests using the combination of P-band backscatter and vegetation height compared to backscatter alone was observed [14,73]. In contrast to P-band, L-band PolInSAR heights play an important role in Remningstorp where R^2 increased from 0.68 (B_1) to 0.8 (B_7), RMSE decreased from 30.2 t ha^{-1} to 24.2 t ha^{-1} and AICc decreased from -51.9 to -68.0. This suggests that a larger range of biomass could be covered in the biomass estimation with L-band SAR than the frequently found saturation limit. Previous studies suggested to overcome the saturation limit utilizing multi-source data and machine learning algorithms [30–32]. The overcoming of the saturation limit with a single data source by combining backscatter and PolInSAR height information could be of significance for future L-band missions, which enable the PolInSAR technique.

As mentioned above, the single source information (backscatter and PolInSAR height from L- and P-band) involve uncertainties. These are for example based on topography (backscatter and height), ground contribution, assumed vertical distribution and baselines in the PolInSAR height retrieval. Consequently, the combination of different predictors might also add disinformation, which could explain the higher RMSE and AICc in Krycklan of the L-band HV backscatter and L-band PolInSAR height (B_7, 19.7%) compared to L-band HV backscatter alone (B_1, 18.8%).

The gains in biomass retrieval accuracy and robustness by including PolInSAR forest heights in the combined regression models are modest when compared to the integration of L- and P-band intensity measurements. This is evident comparing results from model B_4 (intensity only using L- and P-band observables) and model B_{10} which integrates L-band PolInSAR height information. A slightly reduced overall RMSE from 22.8 to 20.8 t ha^{-1} for Remningstorp and no change in the results for Krycklan were observed. The R^2 was similar for the models B_4 and B_{10} in both study areas.

The general study results as discussed above have useful implications for the BIOMASS mission and its objectives. The first is that combining L-band and P-band intensity radar observables can lead to improved and consistent forest biomass information over boreal forests with respect to a single P-band mission. It seems that both bands are complementary in the aboveground biomass estimation of northern latitude forests. This means for instance that one band estimates the biomass more accurate than the other and vice versa depending on the biome and the actual biomass. The ground topography as well as forest structure and thus biomass is different between the two study areas, whereas acquisition conditions and dominating tree species were similar. P-band seems more sensitive to the higher biomass due to its longer wavelength than L-band, whereas L-band is more sensitive to the lower biomass forest. Consequently, the combination complements the biomass prediction to a larger range of biomass. The robustness of the results with respect to the different study areas is especially attractive as the forest biomass conditions on the ground are *a priori* unknown (as it is normally the case) and an ideal single band cannot be selected beforehand.

Given the availability of L-band SAR intensity data over boreal forests this is attractive and further research should be done in order to extend the results in time and space to other study areas and topographic conditions. For instance, the results suggest that the applied topographic correction might be sufficient for the two study areas, which is not necessarily the case for other study areas, where further correction might be necessary by taking for instance the slope angle in azimuth into account. A further implication is that single frequency L-band SAR missions yield similar performances to P-band/L-band intensity results only when combined with height estimates obtained through PolInSAR or other more sophisticated techniques such as TomoSAR. This can be seen for example at the results for L-band model B_8 and B_4 for both study areas. In practice due to the higher temporal decorrelation this implies a single-pass system such as Tandem-L or one based on a passive receive companion satellite flying in convoy to an active master satellite as has been studied by various agencies. This would also provide a mean to extend BIOMASS results to areas not covered by this mission e.g., over North America and Europe due to Space Objects Tracking Radar (SOTR) constraints [5].

It is important to note that these conclusions are based on the available data i.e. the two study areas in Sweden. Further, the aboveground biomass was estimated with an accuracy of less than 21% in the forest of Remningstorp with a stand-level aboveground biomass up to 287 t ha^{-1}. This is close to the global target accuracy of the BIOMASS satellite, which is 20% [5]. Therefore, research should continue to improve the accuracy by e.g., using further topographic correction in order to meet the requested accuracy of BIOMASS. Other studies suggested improved results by combining multi-source data (like L-band SAR and optical) via machine learning or data fusion algorithms [31], which could be assessed in the future also for L- and P-band SAR data. Future work could also concentrate on extending these results to other study areas to verify the generalized conclusions and linking the results to observations through TomoSAR and modelling activities. In addition, a stratification of aboveground biomass could be considered in the combination of the two bands in order to select the ideal band for the actual biomass. In this case, L-band could be used for lower and P-band for higher biomass strata, which would be further combined to a final aboveground biomass information.

6. Conclusions

The results from this study confirm that L-band as well as P-band SAR have high potential to individually estimate forest aboveground biomass. This was investigated in a boreal and a hemi-boreal forest in Sweden with a stand-level aboveground biomass ranging from 28 t ha^{-1} to 183 t ha^{-1} and 11 t ha^{-1} to 287 t ha^{-1}. It is worth noting at the same time that L- and P-band also showed some limitations in terms of retrieval. The L-band to biomass relationship was weaker in higher biomass compared to lower biomass forest, whereas for P-band the opposite was observed. It is worth noting that the PolInSAR height improved the performance of biomass with L-band in Remningstorp, whereas no improvement was observed at P-band in both study areas. However, the combination of both bands resulted in similar or improved aboveground biomass estimation compared to the best results of the individual bands. The results suggest that the combination of L- and P-band has potential to overcome limitations of one band for aboveground biomass estimation, where one band estimates the biomass more accurately than the other and vice versa depending on the actual biomass. This is especially relevant as the forest aboveground biomass conditions and thus, the ideal single band are *a priori* unknown.

Author Contributions: M.S. and M.W.J.D. conceived and designed the experiment; M.S. performed the processing, analyzed the data and wrote the paper; M.W.J.D. provided comments and corrections to the manuscript.

Funding: This research received no external funding

Acknowledgments: This work was prepared under Postdoctoral Research Fellowship Program of ESA. The authors would like to thank the campaign teams of the BioSAR-1 and BioSAR-2 campaign.

Conflicts of Interest: The authors declare no conflict of interest.

References

1. Gibbs, H.K.; Brown, S.; Niles, J.O.; Foley, J.A. Monitoring and estimating tropical forest carbon stocks: Making REDD a reality. *Environ. Res. Lett.* **2007**, *2*, 1–13. [CrossRef]
2. Olander, L.P.; Gibbs, H.K.; Steininger, M.; Swenson, J.J.; Murray, B.C. Reference scenarios for deforestation and forest degradation in support of REDD: A review of data and methods. *Environ. Res. Lett.* **2008**, *3*, 1–11. [CrossRef]
3. Van der Werf, G.R.; Morton, D.C.; DeFries, R.S.; Olivier, J.G.J.; Kasibhatla, P.S.; Jackson, R.B.; Collatz, G.J.; Randerson, J.T. CO_2 emissions from forest loss. *Nat. Geosci.* **2009**, *2*, 737–738. [CrossRef]
4. Martin, A.R.; Thomas, S.C. A Reassessment of Carbon Content in Tropical Trees. *PLoS ONE* **2011**, *6*, e23533, doi:10.1371/journal.pone.0023533. [CrossRef] [PubMed]
5. ESA. *Report for Mission Selection: Biomass, ESA SP-1324/1*; European Space Agency: Nordwijk, The Netherlands, 2012.
6. Le Toan, T.; Quegan, S.; Davidson, M.; Balzter, H.; Paillou, P.; Papathanassiou, K.; Plummer, S.; Rocca, F.; Saatchi, S.; Shugart, H.; et al. The BIOMASS mission: Mapping global forest biomass to better understand the terrestrial carbon cycle. *Remote Sens. Environ.* **2011**, *115*, 2850–2860, doi:10.1016/j.rse.2011.03.020. [CrossRef]
7. Imhoff, M.L. Radar backscatter and biomass saturation: Ramifications for global biomass inventory. *IEEE Trans. Geosci. Remote Sens.* **1995**, *33*, 511–518, doi:10.1109/36.377953. [CrossRef]
8. Villard, L.; Le Toan, T. Relating P-Band SAR Intensity to Biomass for Tropical Dense Forests in Hilly Terrain: y0 or t0? *IEEE J. Sel. Top. Appl. Earth Obs. Remote Sens.* **2015**, *8*, 214–223, doi:10.1109/JSTARS.2014.2359231. [CrossRef]
9. Soja, M.J.; Sandberg, G.; Ulander, L.M.H. Regression-Based Retrieval of Boreal Forest Biomass in Sloping Terrain Using P-Band SAR Backscatter Intensity Data. *IEEE Trans. Geosci. Remote Sens.* **2013**, *51*, 2646–2665, doi:10.1109/TGRS.2012.2219538. [CrossRef]
10. Sandberg, G.; Ulander, L.; Fransson, J.; Holmgren, J.; Toan, T.L. L- and P-band backscatter intensity for biomass retrieval in hemiboreal forest. *Remote Sens. Environ.* **2011**, *115*, 2874–2886, DESDynI VEG-3D Special Issue, doi:10.1016/j.rse.2010.03.018. [CrossRef]

11. Santos, J.R.; Freitas, C.C.; Araujo, L.S.; Dutra, L.V.; Mura, J.C.; Gama, F.F.; Soler, L.S.; Sant'Anna, S.J. Airborne P-band SAR applied to the aboveground biomass studies in the Brazilian tropical rainforest. *Remote Sens. Environ.* **2003**, *87*, 482–493, doi:10.1016/j.rse.2002.12.001. [CrossRef]
12. Hoekman, D.H.; Quinones, M.J. Land cover type and biomass classification using AirSAR data for evaluation of monitoring scenarios in the Colombian Amazon. *IEEE Trans. Geosci. Remote Sens.* **2000**, *38*, 685–696, doi:10.1109/36.841998. [CrossRef]
13. Le Toan, T.; Beaudoin, A.; Riom, J.; Guyon, D. Relating forest biomass to SAR data. *IEEE Trans. Geosci. Remote Sens.* **1992**, *30*, 403–411. [CrossRef]
14. Saatchi, S.; Marlier, M.; Chazdon, R.L.; Clark, D.B.; Russell, A.E. Impact of spatial variability of tropical forest structure on radar estimation of aboveground biomass. *Remote Sens. Environ.* **2011**, *115*, 2836–2849. [CrossRef]
15. Kasischke, E.S.; Melack, J.M.; Dobson, M.C. The use of imaging radars for ecological applications: A review. *Remote Sens. Environ.* **1997**, *59*, 141–156, doi:10.1016/S0034-4257(96)00148-4. [CrossRef]
16. Luckman, A.; Baker, J.; Wegmueller, U. Repeat-Pass Interferometric Coherence Measurements of Disturbed Tropical Forest from JERS and ERS Satellites. *Remote Sens. Environ.* **2000**, *73*, 350–360, doi:10.1016/S0034-4257(00)00110-3. [CrossRef]
17. Saatchi, S.S.; Soares, J.V.; Alves, D.S. Mapping deforestation and land use in amazon rainforest by using SIR-C imagery. *Remote Sens. Environ.* **1997**, *59*, 191–202, doi:10.1016/S0034-4257(96)00153-8. [CrossRef]
18. Naidoo, L.; Mathieu, R.; Main, R.; Kleynhans, W.; Wessels, K.; Asner, G.; Leblon, B. Savannah woody structure modelling and mapping using multi-frequency (X-, C- and L-band) Synthetic Aperture Radar data. *ISPRS J. Photogramm. Remote Sens.* **2015**, *105*, 234–250, doi:10.1016/j.isprsjprs.2015.04.007. [CrossRef]
19. Englhart, S.; Keuck, V.; Siegert, F. Aboveground biomass retrieval in tropical forests—The potential of combined X- and L-band SAR data use. *Remote Sens. Environ.* **2011**, *115*, 1260–1271. [CrossRef]
20. Schlund, M.; von Poncet, F.; Kuntz, S.; Schmullius, C.; Hoekman, D.H. TanDEM-X data for aboveground biomass retrieval in a tropical peat swamp forest. *Remote Sens. Environ.* **2015**, *158*, 255–266, doi:10.1016/j.rse.2014.11.016. [CrossRef]
21. Castro, K.L.; Sanchez-Azofeifa, G.A.; Rivard, B. Monitoring secondary tropical forests using space-borne data: Implications for Central America. *Int. J. Remote Sens.* **2003**, *24*, 1853–1894, doi:10.1080/01431160210154056. [CrossRef]
22. Ranson, K.J.; Sun, G. Mapping biomass of a northern forest using multifrequency SAR data. *IEEE Trans. Geosci. Remote Sens.* **1994**, *32*, 388–396, doi:10.1109/36.295053. [CrossRef]
23. Luckman, A.; Baker, J.; Honzak, M.; Lucas, R. Tropical Forest Biomass Density Estimation Using JERS-1 SAR: Seasonal Variation, Confidence Limits, and Application to Image Mosaics. *Remote Sens. Environ.* **1998**, *63*, 126–139, doi:10.1016/S0034-4257(97)00133-8. [CrossRef]
24. Mitchard, E.; Saatchi, S.; Lewis, S.; Feldpausch, T.; Woodhouse, I.; Sonke, B.; Rowland, C.; Meir, P. Measuring biomass changes due to woody encroachment and deforestation/degradation in a forest-savanna boundary region of central Africa using multi-temporal L-band radar backscatter. *Remote Sens. Environ.* **2011**, *115*, 2861–2873, DESDynI VEG-3D Special Issue. [CrossRef]
25. Gama, F.F.; Dos Santos, J.R.; Mura, J.C. Eucalyptus Biomass and Volume Estimation Using Interferometric and Polarimetric SAR Data. *Remote Sens.* **2010**, *2*, 939–956, doi:10.3390/rs2040939. [CrossRef]
26. Santoro, M.; Beer, C.; Cartus, O.; Schmullius, C.; Shvidenko, A.; McCallum, I.; Wegmüller, U.; Wiesmann, A. Retrieval of growing stock volume in boreal forest using hyper-temporal series of Envisat ASAR ScanSAR backscatter measurements. *Remote Sens. Environ.* **2011**, *115*, 490–507, doi:10.1016/j.rse.2010.09.018. [CrossRef]
27. Yu, Y.; Saatchi, S. Sensitivity of L-Band SAR Backscatter to Aboveground Biomass of Global Forests. *Remote Sens.* **2016**, *8*, 522. [CrossRef]
28. Moreira, A.; Krieger, G.; Hajnsek, I.; Papathanassiou, K.; Younis, M.; Lopez-Dekker, P.; Huber, S.; Villano, M.; Pardini, M.; Eineder, M.; et al. Tandem-L: A Highly Innovative Bistatic SAR Mission for Global Observation of Dynamic Processes on the Earth's Surface. *IEEE Geosci. Remote Sens. Mag.* **2015**, *3*, 8–23, doi:10.1109/MGRS.2015.2437353. [CrossRef]
29. Saatchi, S.S.; Moghaddam, M. Estimation of crown and stem water content and biomass of boreal forest using polarimetric SAR imagery. *IEEE Trans. Geosci. Remote Sens.* **2000**, *38*, 697–709, doi:10.1109/36.841999. [CrossRef]

30. Rodriguez-Veiga, P.; Saatchi, S.; Tansey, K.; Balzter, H. Magnitude, spatial distribution and uncertainty of forest biomass stocks in Mexico. *Remote Sens. Environ.* **2016**, *183*, 265–281, doi:10.1016/j.rse.2016.06.004. [CrossRef]
31. Vafaei, S.; Soosani, J.; Adeli, K.; Fadaei, H.; Naghavi, H.; Pham, T.D.; Bui, D.T. Improving Accuracy Estimation of Forest Aboveground Biomass Based on Incorporation of ALOS-2 PALSAR-2 and Sentinel-2A Imagery and Machine Learning: A Case Study of the Hyrcanian Forest Area (Iran). *Remote Sens.* **2018**, *10*, 172. [CrossRef]
32. Basuki, T.M.; Skidmore, A.K.; Hussin, Y.A.; Duren, I.V. Estimating tropical forest biomass more accurately by integrating ALOS PALSAR and Landsat-7 ETM+ data. *Int. J. Remote Sens.* **2013**, *34*, 4871–4888, doi:10.1080/01431161.2013.777486. [CrossRef]
33. Hame, T.; Rauste, Y.; Antropov, O.; Ahola, H.; Kilpi, J. Improved Mapping of Tropical Forests With Optical and SAR Imagery, Part II: Above Ground Biomass Estimation. *IEEE J. Sel. Top. Appl. Earth Obs. Remote Sens.* **2013**, *6*, 92–101, doi:10.1109/JSTARS.2013.2241020. [CrossRef]
34. Papathanassiou, K.; Cloude, S. Single-baseline polarimetric SAR interferometry. *IEEE Trans. Geosci. Remote Sens.* **2001**, *39*, 2352–2363, doi:10.1109/36.964971. [CrossRef]
35. Hajnsek, I.; Kugler, F.; Lee, S.K.; Papathanassiou, K. Tropical-Forest-Parameter Estimation by Means of Pol-InSAR: The INDREX-II Campaign. *IEEE Trans. Geosci. Remote Sens.* **2009**, *47*, 481–493, doi:10.1109/TGRS.2008.2009437. [CrossRef]
36. Koch, B. Status and future of laser scanning, synthetic aperture radar and hyperspectral remote sensing data for forest biomass assessment. *ISPRS J. Photogramm. Remote Sens.* **2010**, *65*, 581–590. [CrossRef]
37. Neumann, M.; Saatchi, S.S.; Ulander, L.M.H.; Fransson, J.E.S. Assessing Performance of L- and P-Band Polarimetric Interferometric SAR Data in Estimating Boreal Forest Above-Ground Biomass. *IEEE Trans. Geosci. Remote Sens.* **2012**, *50*, 714–726, doi:10.1109/TGRS.2011.2176133. [CrossRef]
38. Lu, D.; Chen, Q.; Wang, G.; Liu, L.; Li, G.; Moran, E. A survey of remote sensing-based aboveground biomass estimation methods in forest ecosystems. *Int. J. Digit. Earth* **2016**, *9*, 63–105, doi:10.1080/17538947.2014.990526. [CrossRef]
39. Zhao, P.; Lu, D.; Wang, G.; Liu, L.; Li, D.; Zhu, J.; Yu, S. Forest aboveground biomass estimation in Zhejiang Province using the integration of Landsat TM and ALOS PALSAR data. *Int. J. Appl. Earth Obs. Geoinf.* **2016**, *53*, 1–15, doi:10.1016/j.jag.2016.08.007. [CrossRef]
40. Hajnsek, I.; Scheiber, R.; Ulander, L.; Gustavsson, A.; Sandberg, G.; Tebaldini, S.; Guarnieri, A.M.; Rocca, F.; Bombardini, F.; Pardini, M. *BIOSAR 2007—Technical Assistance for the Development of Airborne SAR and Geophysical Measurements during the BioSAR 2007 Experiment*; Final Report; ESA: Paris, France, 2008; Volume 1.
41. Hajnsek, I.; Scheiber, R.; Keller, M.; Horn, R.; Lee, S.; Ulander, L.; Gustavsson, A.; Sandberg, G.; Le Toan, T.; Tebaldini, S.; et al. *BIOSAR 2008—Technical Assistance for the Development of Airborne SAR and Geophysical Measurements during the BioSAR 2008 Experiment*; Final Report; ESA: Paris, France, 2009; Volume 1.
42. Hoekman, D.H.; Reiche, J. Multi-model radiometric slope correction of SAR images of complex terrain using a two-stage semi-empirical approach. *Remote Sens. Environ.* **2015**, *156*, 1–10, doi:10.1016/j.rse.2014.08.037. [CrossRef]
43. Ulander, L.M.H. Radiometric slope correction of synthetic-aperture radar images. *IEEE Trans. Geosci. Remote Sens.* **1996**, *34*, 1115–1122, doi:10.1109/36.536527. [CrossRef]
44. Van Zyl, J.J. The effect of topography on radar scattering from vegetated areas. *IEEE Trans. Geosci. Remote Sens.* **1993**, *31*, 153–160, doi:10.1109/36.210456. [CrossRef]
45. Hallberg, B.; Smith-Jonforsen, G.; Ulander, L.M.H.; Sandberg, G. A Physical-Optics Model for Double-Bounce Scattering From Tree Stems Standing on an Undulating Ground Surface. *IEEE Trans. Geosci. Remote Sens.* **2008**, *46*, 2607–2621, doi:10.1109/TGRS.2008.919271. [CrossRef]
46. Horn, B.K.P. Hill shading and the reflectance map. *Proc. IEEE* **1981**, *69*, 14–47, doi:10.1109/PROC.1981.11918. [CrossRef]
47. Hoekman, D.H. Radar Remote Sensing Data for Applications in Forestry. Ph.D. Thesis, Wageningen Agricultural University, Wageningen, The Netherlands, 1990.
48. Goering, D.J.; Chen, H.; Hinzman, L.D.; Kane, D.L. Removal of terrain effects from SAR satellite imagery of Arctic tundra. *IEEE Trans. Geosci. Remote Sens.* **1995**, *33*, 185–194, doi:10.1109/36.368210. [CrossRef]
49. Cloude, S.; Papathanassiou, K. Polarimetric SAR interferometry. *IEEE Trans. Geosci. Remote Sens.* **1998**, *36*, 1551–1565, doi:10.1109/36.718859. [CrossRef]

50. Cloude, S.; Papathanassiou, K. Three-stage inversion process for polarimetric SAR interferometry. *IEE Proc. Radar Sonar Navig.* **2003**, *150*, 125–134, doi:10.1049/ip-rsn:20030449. [CrossRef]
51. Kugler, F.; Lee, S.K.; Hajnsek, I.; Papathanassiou, K.P. Forest Height Estimation by Means of Pol-InSAR Data Inversion: The Role of the Vertical Wavenumber. *IEEE Trans. Geosci. Remote Sens.* **2015**, *53*, 5294–5311, doi:10.1109/TGRS.2015.2420996. [CrossRef]
52. Treuhaft, R.N.; Madsen, S.N.; Moghaddam, M.; van Zyl, J.J. Vegetation characteristics and underlying topography from interferometric radar. *Radio Sci.* **1996**, *31*, 1449–1485, doi:10.1029/96RS01763. [CrossRef]
53. Treuhaft, R.N.; Siqueira, P.R. Vertical structure of vegetated land surfaces from interferometric and polarimetric radar. *Radio Sci.* **2000**, *35*, 141–177, doi:10.1029/1999RS900108. [CrossRef]
54. Lee, S.K.; Kugler, F.; Papathanassiou, K.; Hajnsek, I. Multibaseline Polarimetric SAR Interferometry Forest Height Inversion Approaches. In Proceedings of the ESA POLinSAR Workshop, Frascati, Italy, 24–28 January 2011.
55. Rignot, E.; Way, J.; Williams, C.; Viereck, L. Radar estimates of aboveground biomass in boreal forests of interior Alaska. *IEEE Trans. Geosci. Remote Sens.* **1994**, *32*, 1117–1124, doi:10.1109/36.312903. [CrossRef]
56. Fransson, J.E.S. Estimation of stem volume in boreal forests using ERS-1 C- and JERS-1 L-band SAR data. *Int. J. Remote Sens.* **1999**, *20*, 123–137, doi:10.1080/014311699213640. [CrossRef]
57. Tebaldini, S.; Rocca, F. Multibaseline Polarimetric SAR Tomography of a Boreal Forest at P- and L-Bands. *IEEE Trans. Geosci. Remote Sens.* **2012**, *50*, 232–246, doi:10.1109/TGRS.2011.2159614. [CrossRef]
58. Ulaby, F.T.; Held, D.; Donson, M.C.; McDonald, K.C.; Senior, T.B.A. Relating Polaization Phase Difference of SAR Signals to Scene Properties. *IEEE Trans. Geosci. Remote Sens.* **1987**, *GE-25*, 83–92, doi:10.1109/TGRS.1987.289784. [CrossRef]
59. Skriver, H.; Svendsen, M.T.; Thomsen, A.G. Multitemporal C- and L-band polarimetric signatures of crops. *IEEE Trans. Geosci. Remote Sens.* **1999**, *37*, 2413–2429, doi:10.1109/36.789639. [CrossRef]
60. Askne, J.I.; Fransson, J.E.; Santoro, M.; Soja, M.J.; Ulander, L.M. Model-Based Biomass Estimation of a Hemi-Boreal Forest from Multitemporal TanDEM-X Acquisitions. *Remote Sens.* **2013**, *5*, 5574–5597, doi:10.3390/rs5115574. [CrossRef]
61. Solberg, S.; Astrup, R.; Breidenbach, J.; Nilsen, B.; Weydahl, D. Monitoring spruce volume and biomass with InSAR data from TanDEM-X. *Remote Sens. Environ.* **2013**, *139*, 60–67, doi:10.1016/j.rse.2013.07.036. [CrossRef]
62. Soja, M.; Persson, H.; Ulander, L. Estimation of Forest Biomass From Two-Level Model Inversion of Single-Pass InSAR Data. *IEEE Trans. Geosci. Remote Sens.* **2015**, *53*, 5083–5099, doi:10.1109/TGRS.2015.2417205. [CrossRef]
63. Caicoya, A.T.; Kugler, F.; Hajnsek, I.; Papathanassiou, K.P. Large-Scale Biomass Classification in Boreal Forests With TanDEM-X Data. *IEEE Trans. Geosci. Remote Sens.* **2016**, *54*, 5935–5951, doi:10.1109/TGRS.2016.2575542. [CrossRef]
64. Seber, G.A.F.; Lee, A.J. *Linear Regression Analysis*; Wiley & Sons: Hoboken, NJ, USA, 2003.
65. Chambers, J.M. Linear models. In *Statistical Models in S*; Chambers, J.M., Hastie, T.J., Eds.; Wadsworth & Brooks/Cole Advanced Books & Software: Pacific Grove, CA, USA, 1992.
66. Schlund, M.; Scipal, K.; Davidson, M.W. Forest classification and impact of BIOMASS resolution on forest area and aboveground biomass estimation. *Int. J. Appl. Earth Obs. Geoinf.* **2017**, *56*, 65–76, doi:10.1016/j.jag.2016.12.001. [CrossRef]
67. Newman, M. Regression Analysis of log-transformed data: Statistical bias and its correction. *Environ. Toxicol. Chem.* **1993**, *12*, 1129–1133. [CrossRef]
68. Breiman, L.; Friedman, J.; Stone, C.J.; Olshen, R.A. *Classification and Regression Trees*; CRC Press: Wadsworth, IL, USA, 1984.
69. Kohavi, R. A study of cross-validation and bootstrap for accuracy estimation and model selection. *IJCAI* **1995**, *14*, 1137–1145.
70. Burnham, K.P.; Anderson, D.R. *Model Selection and Multimodel Inference: A Practical Information-Theoretic Approach*, 2nd ed.; Springer: Berlin/Heidelberg, Germany, 2002; doi:10.1007/b97636.
71. Spiess, A.N.; Neumeyer, N. An evaluation of R2 as an inadequate measure for nonlinear models in pharmacological and biochemical research: A Monte Carlo approach. *BMC Pharmacol.* **2010**, *10*, 6. [CrossRef] [PubMed]

72. Mette, T.; Kugler, F.; Papathanassiou, K.; Hajnsek, I. Forest and the Random Volume over Ground-nature and effect of 3 possible error types. In Proceedings of the EUSAR 2006: 6th European Conference on Synthetic Aperture Radar, Dresden, Germany, 16–18 May 2006, pp. 1–4.
73. Neeff, T.; Dutra, L.V.; dos Santos, J.R.; Freitas, C.d.C.; Araujo, L.S. Tropical Forest Measurement by Interferometric Height Modeling and P-Band Radar Backscatter. *Forest Sci.* **2005**, *51*, 585–594.